IEEE Access
Multidisciplinary ⋮ Rapid Review ⋮ Open Access Journal

Received 20 October 2022, accepted 13 November 2022, date of publication 18 November 2022,
date of current version 23 November 2022.

*Digital Object Identifier 10.1109/ACCESS.2022.3223476*

RESEARCH ARTICLE

# Optimal Hydrogen Production and High Efficient Output Smoothing in Wind Farm

**KENTA KOIWA, (Member, IEEE), LINMAN CUI, TADANAO ZANMA, (Member, IEEE), AND KANG-ZHI LIU, (Senior Member, IEEE)**
Department of Electrical and Electronic Engineering, Chiba University, Chiba 263-8522, Japan
Corresponding author: Kenta Koiwa (kenta.koiwa@chiba-u.jp)

This work was supported by JSPS KAKENHI under Grant JP22K14233.

**ABSTRACT** This paper proposes a novel optimal control method for integrated systems of Wind farms (WFs) and hydrogen production systems (HPSs). Green hydrogen production via renewable power generation (RPG), such as wind power generation, is a promising technology to overcome environmental problems. RPG has the potential to become more widespread if we can produce hydrogen in an HPS using the output fluctuation and the output surplus of RPG, which cause power outages due to supply-demand imbalances. The proposed optimal control maximizes the capacity factor of HPS while producing hydrogen constantly and satisfying the technical requirement related to the output fluctuation of the WF. The proposed control is also easy to implement and needs no WF output forecast. We demonstrate the effectiveness of the proposed optimal control through simulated comparative analysis with conventional methods.

**INDEX TERMS** Electrolyzer, output smoothing, hydrogen production, wind generation.

## I. INTRODUCTION

Hydrogen is an essential energy source in many applications, such as fuel cell vehicles, hydrogen-powered heavy-duty trucks, household and industrial fuel cells (FCs) [1], [2], [3]. Moreover, valuable chemicals such as methane can be generated by blending hydrogen with carbon dioxide [4]. Thus, hydrogen is frequently credited as an alternative source to fossil fuels.

Green hydrogen production via renewable power generation (RPG), such as photovoltaic and wind power generation, is a promising technology to prevent environmental problems, as hydrogen can be produced without carbon dioxide [5], [6]. For green hydrogen production, there are two types of systems consisting of RPG and hydrogen production systems (HPSs): stand-alone systems [7], [8] and grid-connected systems [9], [10], [11], [12]. In the grid-connected systems, power can be supplied to the grid while producing hydrogen in the HPS. Moreover, RPG has the potential to become more widespread if we can produce hydrogen in the HPS using output fluctuation and output surplus of RPG, which cause power outages due to supply-demand imbalances [9], [10], [11], [12].

The associate editor coordinating the review of this manuscript and approving it for publication was Inam Nutkani.

In grid-connected systems, it is important to mitigate RPG output fluctuation, produce hydrogen constantly, and maintain a high capacity factor of HPS. To achieve these purposes simultaneously, some methods have been proposed. In [13], an output smoothing method for RPGs by combining HPSs and FCs was proposed. In [14] and [15], a system composed of HPSs, FCs, and super-capacitors was proposed. Since the HPS produces hydrogen by consuming electrical power and the FC generates power by consuming hydrogen, the combination of HPSs and FCs can operate like a battery and smooth the RPG output. However, the energy conversion between hydrogen and electricity in the combination of HPSs and FCs induces the loss [10]. In addition, it is difficult to store hydrogen for applications such as fuel cell vehicles if the hydrogen itself is used to mitigate RPG output fluctuation. In [16], the output smoothing of wind turbines was investigated by utilizing wind power forecasting in a system composed of HPSs, FCs, and batteries. This method can also smooth wind turbine output. Nevertheless, no discussion has been found about constant hydrogen production and improvement of the capacity factor of HPS. Optimization methods based on model predictive control for a microgrid containing RPG, HPSs, FCs, and batteries were proposed in [17] and [18]. The components in the microgrids optimally operates based on the model predictive control, minimizing the operation cost. However, these methods require high calculation power for

online complex optimization. In addition, the initial costs are high, and the energy conversion loss is inevitable since they utilize batteries and FCs [17] and [18].

Smoothing control methods using HPSs for RPG without batteries or FCs were investigated in [9], [10], and [12]. In [9] and [10], controllers based on the low-pass filter (LPF), which is usually used in energy storage systems (ESSs), were proposed. Nevertheless, their controllers cannot mitigate the output fluctuation of the RPG sufficiently since the HPS cannot discharge, unlike the ESS. Moreover, it is difficult to increase the capacity factor of HPS and produce hydrogen constantly with the methods in [9] and [10] since they produce hydrogen utilizing only the output fluctuation of the RPG and require a high rated power of the HPS to consume the large output fluctuation. In other words, these two methods cannot produce hydrogen when the output of the RPG is constant.

To overcome these disadvantages in the methods proposed in [9] and [10], we proposed a coordinated control method for an integrated system of wind farm (WF) and HPS [12]. Virtual discharge in the HPS and kinetic energy control of the WF enable us to smooth the output fluctuation of WF sufficiently while maintaining a high capacity factor of HPS [12]. However, the performance of HPS and WF is limited because the controller uses an LPF which is a type of linear control. In other words, there is room for improvement in the efficiency of WF and capacity factor of HPS.

This paper proposes a novel optimal control for integrated systems of the WF and the HPS. Specifically, we focus on wind power generation due to advantages such as cost-effectiveness and power generation during the day or night [4], [19]. In the proposed optimal control, kinetic energy of wind turbines is utilized to smooth the output fluctuation [12]. The proposed optimal control maximizes the capacity factor of HPS while producing hydrogen constantly and satisfying the technical requirement related to the output fluctuation of the WF. Moreover, the proposed controller is easy to implement, and requires no WF output forecast.

The contributions of this paper are summarized as follows:

1) The proposed optimal control enables us to produce more hydrogen in an HPS with lower-rated power than conventional methods. The technical requirement can also be handled directly as a constraint. Consequently, the proposed approach can achieve constant hydrogen production, mitigation of the output fluctuation of WF, and high capacity factor of HPS.

2) No high-grade computation device is required in the proposed optimal control since the optimal references of the HPS and the WF can be calculated without any complex algorithm. In addition, no design parameters are included in the proposed controller. Thus, it can be easily implemented.

3) The conservativeness in a linear control is mitigated in the proposed control since no LPF is included in the proposed controller. Therefore, the proposed control can improve the efficiency of WF and the capacity factor of HPS although it is inevitable to degrade the efficiency of WF when kinetic energy is used to smooth output fluctuations.

**TABLE 1. Notations.**

| | |
|---|---|
| WG and WF | |
| $P$ | WG output |
| $P_{\mathrm{WF}}$ $(=\sum_{i=1}^{n} P_i)$ | WF output |
| $P^{\dagger}$ | MPPT output reference |
| $P_{\mathrm{g}}(=P_{\mathrm{WF}}-P_{\mathrm{H}})$ | Power supplied to grid |
| $\hat{P}$ | Captured wind power |
| $\rho$ $(\approx 1.225\ \mathrm{kg/m^3})$ | Air density |
| $R$ | Blade radius |
| $V$ | Wind speed |
| $C_{\mathrm{p}}$ | Power coefficient |
| $\beta$ | Blade pitch angle |
| $\lambda$ | Tip speed ratio |
| $\omega$ | Rotor angular frequency |
| $H_{\mathrm{J}}$ $(=3\ \mathrm{s})$ | Inertia constant |
| HPS | |
| $P_{\mathrm{H}}$ | Power supplied to AC-DC converter |
| $\hat{P}_{\mathrm{H}}$ | Consumed power in HPS |
| $H$ | Hydrogen gas flow rate |
| $\eta$ | Overall converter efficiency |
| $V_{\mathrm{dc}}$ | Output voltage in DC-DC converter |
| $I_{\mathrm{dc}}$ | Output current in DC-DC converter |
| Subscripts | |
| pu | Per-unit |
| $i=1,2,\ldots,n$ | Number of WG |
| Superscripts | |
| ref | Reference |
| n | Rated value |

We demonstrate the effectiveness of the proposed optimal control through comparative analysis with the methods proposed in [9], [10], and [12] via simulations.

The rest of this paper is organized as follows: Section II describes the system configuration, wind turbine model, electrolyzer (ELZ) model, and technical requirement. Section III presents the proposed optimal control for an integrated system of the WF and the HPS. Section IV demonstrates the effectiveness of the proposed optimal control through simulations, and lastly, section V concludes this paper.

## II. PRELIMINARIES

Table 1 lists the main notations used in this paper. The continuous-time signal $x(t)$ and discrete-time signal $x[k]$ are simply denoted by $x$ when it is clear from the context.[1]

### A. SYSTEM CONFIGURATION

Fig. 1 shows the system configuration addressed in this paper, and Fig. 2 shows its block diagram. We assume that the wind generator (WG) is composed of a variable speed wind turbine, such as a permanent magnet synchronous generator. The HPS is connected to the grid through AC-DC and DC-DC converters. As listed in Table 1, for example, $P_{\mathrm{H}}^{\mathrm{ref}}$, $P_{i\mathrm{pu}}$ $(i=1,2,\ldots,n)$, and $P_i^{\mathrm{n}}$ $(i=1,2,\ldots,n)$ are the reference power for the AC-DC converter in the HPS, the per-unit power of the $i$-th WG, and the rated power of the $i$-th WG, respectively. In the Optimization block shown in Fig. 2, $P_i^{\mathrm{ref}}$ $(i=1,2,\ldots,n)$ and $P_{\mathrm{H}}^{\mathrm{ref}}$ are generated to operate the WGs and the HPS optimally. The dynamics of the AC-DC and DC-DC converters can be ignored since their response speed

[1]For simplicity, $x[k]=x(kT_{\mathrm{s}})$ where $k$ is the sample number and $T_{\mathrm{s}}$ is the sampling period.

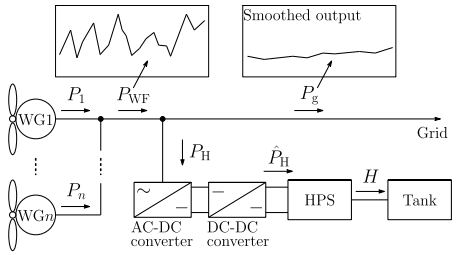


**FIGURE 1.** System configuration.

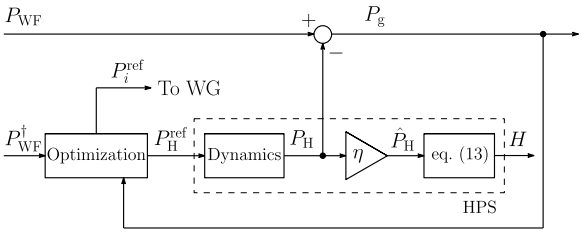


**FIGURE 2.** System block diagram.

is sufficiently fast [10], [15]. Namely, we assume $P_{\mathrm{H}}^{\mathrm{ref}} \approx P_{\mathrm{H}}$. Note that the efficiency of the converters is denoted by $\eta$, as shown in Fig. 2. The positive sign of $P_{\mathrm{H}}$ represents power consumption.

### B. WIND TURBINE MODEL

We briefly describe the wind turbine model used in this paper (See [12] and [20] for more details).

The output characteristics of $i$-th ($i = 1, \ldots, n$) WG is given by

$$\hat{P}_i = \frac{1}{2}\rho\pi R^2 V_i^3 C_{\mathrm{p}i}(\beta_i, \lambda_i), \tag{1}$$

$$C_{\mathrm{p}i}(\lambda_i, \beta_i) = 0.5176\left(\frac{116}{\hat{\lambda}_i} - 0.4\beta_i - 5\right)\mathrm{e}^{\frac{-21}{\hat{\lambda}_i}} + 0.0068\lambda_i, \tag{2}$$

$$\frac{1}{\hat{\lambda}_i} = \frac{1}{\lambda_i + 0.08\beta_i} - \frac{0.035}{\beta_i^3 + 1}, \tag{3}$$

$$\lambda_i = \frac{\omega_i R}{V_i}, \tag{4}$$

$$\omega_{i\mathrm{pu}}\frac{\mathrm{d}\omega_{i\mathrm{pu}}}{\mathrm{d}t} = \frac{1}{2H_{\mathrm{J}}}\hat{P}_{i\mathrm{pu}} - P_{i\mathrm{pu}}, \quad (i = 1, \ldots, n). \tag{5}$$

In this paper, we assume $P_i^{\mathrm{ref}} \approx P_i$ ($i = 1, \ldots, n$) to shorten the simulation time. This assumption is valid since the response speed of the back-to-back converter in the WG is sufficiently fast [12]. Moreover, a pitch angle control system [21] is used in this model.

The $i$-th ($i = 1, \ldots, n$) output reference $P_i^{\dagger}$ at maximum power point tracking (MPPT) and its per-unit value are given, respectively, by

$$P_i^{\dagger} = \frac{1}{2}\rho\pi R^2\left(\frac{R}{\lambda^{\dagger}}\right)^3 C_{\mathrm{p}}^{\dagger}\omega_i^3, \tag{6}$$

$$P_{i\mathrm{pu}}^{\dagger} = \frac{P_i^{\dagger}}{P^{\mathrm{n}}} = \omega_{i\mathrm{pu}}^3, \quad (i = 1, \ldots, n), \tag{7}$$

where $\lambda^{\dagger} = 8.1$, $C_{\mathrm{p}}^{\dagger} = 0.48$, and $P^{\mathrm{n}} = \frac{1}{2}\rho\pi R^2\left(\frac{R}{\lambda^{\dagger}}\right)^3 C_{\mathrm{p}}^{\dagger}(\omega^{\mathrm{n}})^3$. From (7), the MPPT is achieved when $P_{i\mathrm{pu}}^{\mathrm{ref}} = P_{i\mathrm{pu}}^{\dagger}$ ($i = 1, \ldots, n$).

Variable speed wind turbines store (release) kinetic energy in the rotor by adjusting $P_i^{\mathrm{ref}}$ ($i = 1, \ldots, n$). For instance, the rotor accelerates (decelerates) when $P_i^{\mathrm{ref}} < P_i^{\dagger}$ ($P_i^{\mathrm{ref}} > P_i^{\dagger}$) ($i = 1, \ldots, n$). The output fluctuation of the WF can be mitigated by utilizing the kinetic energy [22], [23]. The output reference of the WG to utilize kinetic energy is given by

$$P_i^{\mathrm{ref}} = P_i^{\dagger} - P_i^{\mathrm{k}} \quad (i = 1, \ldots, n), \tag{8}$$

where $P_i^{\mathrm{k}}$ ($i = 1, \ldots, n$) is the kinetic output reference to store (release) kinetic energy in the rotor. It is clear from (8) that the output fluctuation of the WG can be smoothed by adjusting $P_i^{\mathrm{k}}$ ($i = 1, \ldots, n$), although the WG operates off the MPPT. Note that the WG stops when the excess kinetic energy is released. To prevent this, we limit $P_i^{\mathrm{k}}$ ($i = 1, \ldots, n$) as follows:

$$0 \le P_i^{\mathrm{k}} \le P_i^{\dagger} \quad (i = 1, \ldots, n). \tag{9}$$

The WF kinetic output reference $P_{\mathrm{WF}}^{\mathrm{k}}$ given by

$$P_{\mathrm{WF}}^{\mathrm{k}} = \sum_{i=1}^{n} P_i^{\mathrm{k}}. \tag{10}$$

From (9), $P_{\mathrm{WF}}^{\mathrm{k}}$ is also limited as follows:

$$0 \le P_{\mathrm{WF}}^{\mathrm{k}} \le P_{\mathrm{WF}}^{\dagger}, \tag{11}$$

where $P_{\mathrm{WF}}^{\dagger} = \sum_{i=1}^{n} P_i^{\dagger}$ is the WF output obtained by the MPPT.

To evaluate the efficiency of WF as it utilize kinetic energy, we define the efficiency of WF as

$$\text{Efficiency} = \frac{\int_0^{T_{\mathrm{R}}} P_{\mathrm{WF}}\,\mathrm{d}t}{\int_0^{T_{\mathrm{R}}} P_{\mathrm{WF}}^{\dagger}\,\mathrm{d}t} \times 100\%, \tag{12}$$

where $T_{\mathrm{R}}$ is the evaluation period.

### C. ELECTROLYZER MODEL

HPSs are composed of ELZs. We briefly describe the ELZ model used in this paper (See [12], [24], [25] for details).

Fig. 3 shows the electrical ELZ model, composed of one diode, one resistor $R_0$, and one internal voltage $E_0$ [25]. Fig. 4 shows the characteristics of a single ELZ module, as used in this paper. Table 2 lists the specifications of the ELZ module. With a simple calculation using Figs. 3 and 4, we obtain a simplified megawatt-scale HPS model constructed by connecting modules of the ELZ in series and parallel as follows [12], [26]:

$$H = \begin{cases} H^{\dagger} & (H^{\dagger} \ge 0), \\ 0 & (H^{\dagger} < 0), \end{cases} \tag{13}$$

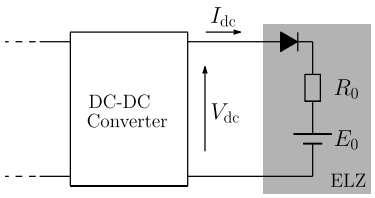


**FIGURE 3.** Electrical ELZ model.

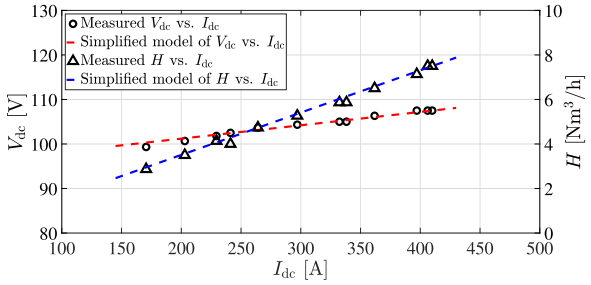


**FIGURE 4.** Characteristics of a single ELZ module [24].

where

$$H^{\dagger} = n_s n_p n_h \left( 0.019 \left( \frac{-E_0 + \sqrt{E_0^2 + 4R_0 \left( \frac{\hat{P}_H}{n_h} \right)}}{2R_0 n_p} \right) - 0.29 \right), \tag{14}$$

and $\hat{P}_H = \eta P_H$ as shown in Fig. 2. In (14), $n_s$ is the number of cascaded ELZ modules in an HPS, and $n_p$ is the parallel number of the cascaded ELZ modules in the HPS, and $n_h$ is the number of HPSs connected in parallel. From (13) and (14), we can calculate $H$ from $P_H$. Note that $P_H$ is limited since the HPS only consumes power, which is described by

$$0 \le P_H \le P_H^n. \tag{15}$$

To evaluate the performance of HPS, we define the capacity factor of HPS as

$$\text{Capacity factor} = \frac{\int_0^{T_R} H \, dt}{\int_0^{T_R} H^n \, dt} \times 100\%. \tag{16}$$

### D. TECHNICAL REQUIREMENT

The fluctuation ratio of $P_g$ in an $h$-second window is defined as [27], [28]

$$\Delta F_g(t; h) = \frac{\max_{t-h \le \tau \le t} P_g(\tau) - \min_{t-h \le \tau \le t} P_g(\tau)}{P_{WF}^n}. \tag{17}$$

Some countries have issued technical requirements for this fluctuation [27], [28], [29]. Fig. 5 illustrates an example. The technical requirement is given by

$$\Delta F_g(t; h) \le \gamma_h, \tag{18}$$

where $\gamma_h \ge 0$ denotes the allowable fluctuation level in the $h$-second window. In (18), $h$ and $\gamma_h$ are given by the technical requirement [27]. For example, if $h = 300$ s and $\gamma_h = 0.1$,

**TABLE 2.** Specifications of a single ELZ module.

| | |
|---|---|
| Rated power | 44.075 kW |
| Rated voltage | 107.5 V |
| Rated current | 410 A |
| Rated gas flow rate | 7.5 Nm$^3$/h |
| $R_0$ | 0.03 Ω |
| $E_0$ | 95.2 V |

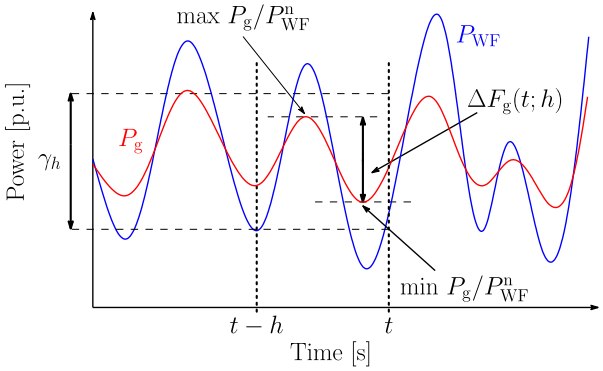


**FIGURE 5.** Technical requirement [28].

the error between the maximum and minimum WF output in a period of 300 s must be suppressed within 0.1 p.u. to satisfy the technical requirement.

In discrete time, (17) and (18) can be rewritten, respectively, as follows [27], [28]:

$$\Delta F_g[k; \hat{h}] = \frac{\max_{k-\hat{h} \le \kappa \le k} P_g[\kappa] - \min_{k-\hat{h} \le \kappa \le k} P_g[\kappa]}{P_{WF}^n}, \tag{19}$$

and

$$\Delta F_g[k; \hat{h}] \le \gamma_h, \tag{20}$$

where $\hat{h} = \lceil h/T_s \rceil$ is the total number of samples in the $h$-second window. Note that $T_s$ is determined such that $T_s \le h$. In subsequent discussion, we rewrite (20) as follows:

$$\underline{\Gamma}[k; \hat{h}, \gamma_h] \le P_{WF}^k[k] + P_H[k] \le \overline{\Gamma}[k; \hat{h}, \gamma_h]. \tag{21}$$

See Appendix A for $\underline{\Gamma}[k; \hat{h}, \gamma_h]$, $\overline{\Gamma}[k; \hat{h}, \gamma_h]$, and (21).

## III. PROPOSED OPTIMAL CONTROL METHOD

We present a novel optimal control method for the integrated system of the WF and the HPS. The aim of the proposed control is to generate the references of power for the AC-DC converter in the HPS and the WF kinetic output, i.e., $P_H^{ref}$ and $P_{WF}^k$ such that the following performances are simultaneously achieved:

A-1) constant hydrogen production in the HPS,
A-2) high capacity factor of HPS,
A-3) improvement of the efficiency of WF as it utilizes kinetic energy, and
A-4) guarantee of the technical requirement given by (18).

We derive the optimal HPS and WF kinetic output references at $k$ that achieve A-1) to A-4), denoted by $P_{H,opt}^{ref}[k]$

and $P^{\mathrm{k}}_{\mathrm{WF,opt}}[k]$, respectively, as the solution of the proposed following constrained optimization problem:

$$(P^{\mathrm{ref}}_{\mathrm{H,opt}}[k],\, P^{\mathrm{k}}_{\mathrm{WF,opt}}[k]) = \underset{P^{\mathrm{ref}}_{\mathrm{H}}[k],\, P^{\mathrm{k}}_{\mathrm{WF}}[k]}{\operatorname{argmin}} \; J(P^{\mathrm{ref}}_{\mathrm{H}}[k], P^{\mathrm{k}}_{\mathrm{WF}}[k]) \quad (22)$$

subject to

$$0 \le P^{\mathrm{k}}_{\mathrm{WF}}[k] \le P^{\dagger}_{\mathrm{WF}}, \quad (23)$$

$$0 \le P^{\mathrm{ref}}_{\mathrm{H}}[k] \le P^{\mathrm{n}}_{\mathrm{H}}, \quad (24)$$

$$\underline{\Gamma}[k;\hat{h},\gamma_h] \le P^{\mathrm{k}}_{\mathrm{WF}}[k] + P^{\mathrm{ref}}_{\mathrm{H}}[k] \le \overline{\Gamma}[k;\hat{h},\gamma_h]. \quad (25)$$

where

$$J(P^{\mathrm{ref}}_{\mathrm{H}}, P^{\mathrm{k}}_{\mathrm{WF}}) = (P^{\mathrm{n}}_{\mathrm{H}} - P^{\mathrm{ref}}_{\mathrm{H}})^2 + (P^{\mathrm{k}}_{\mathrm{WF}})^2. \quad (26)$$

In the first term on the right-hand side of (26), A-1) and A-2) are considered. Meanwhile, A-3) is taken into account in the second term where the kinetic output reference is evaluated. The constraints represented by (11), (15), and (21) related to A-4) are also addressed by (23), (24), and (25), respectively, in the optimization problem.

Fig. 6 shows the three-dimensional plot of (26), and Fig. 7 shows its contour. In Fig. 7, the dashed lines $\overline{L}$ and $\underline{L}$ are described, respectively, as

$$\overline{L} : P^{\mathrm{k}}_{\mathrm{WF}} + P^{\mathrm{ref}}_{\mathrm{H}} - \overline{\Gamma}[k;\hat{h},\gamma_h] = 0, \quad (27)$$

$$\underline{L} : P^{\mathrm{k}}_{\mathrm{WF}} + P^{\mathrm{ref}}_{\mathrm{H}} - \underline{\Gamma}[k;\hat{h},\gamma_h] = 0. \quad (28)$$

Moreover, the shaded region in Fig. 7 shows the region satisfying (23), (24), and (25). From Figs. 6 and 7, the tuple of $(P^{\mathrm{ref}}_{\mathrm{H,opt}}[k], P^{\mathrm{k}}_{\mathrm{WF,opt}}[k])$ is given by

$$(P^{\mathrm{ref}}_{\mathrm{H,opt}}[k], P^{\mathrm{k}}_{\mathrm{WF,opt}}[k]) = \begin{cases} (P^{\mathrm{n}}_{\mathrm{H}}, \underline{\Gamma}[k;\hat{h},\gamma_h] - P^{\mathrm{n}}_{\mathrm{H}}) & (P^{\mathrm{n}}_{\mathrm{H}} \le \underline{\Gamma}[k;\hat{h},\gamma_h]), \\ (P^{\mathrm{n}}_{\mathrm{H}}, 0) & (\underline{\Gamma}[k;\hat{h},\gamma_h] \le P^{\mathrm{n}}_{\mathrm{H}} \le \overline{\Gamma}[k;\hat{h},\gamma_h]), \\ (\overline{\Gamma}[k;\hat{h},\gamma_h], 0) & (\overline{\Gamma}[k;\hat{h},\gamma_h] \le P^{\mathrm{n}}_{\mathrm{H}}). \end{cases} \quad (29)$$

Once $P^{\mathrm{k}}_{\mathrm{WF,opt}}[k]$ is available, the $i$-th ($i = 1, 2, \ldots, n$) WG kinetic output reference $P^{\mathrm{k}}_{i,\mathrm{opt}}[k]$ is given as follows [23]:

$$P^{\mathrm{k}}_{i,\mathrm{opt}}[k] = \frac{P^{\dagger}_{i}[k]}{P^{\dagger}_{\mathrm{WF}}[k]} P^{\mathrm{k}}_{\mathrm{WF,opt}}[k] \quad (i = 1, 2, \ldots, n). \quad (30)$$

It is clear from (29) that the proposed control can easily find the optimal references that achieve A-1) to A-4) without any complex calculation. In addition, the proposed method is free from tuning parameters such as LPF time constants and weights in typical optimization problems. Consequently, the proposed method has significant advantages for constant hydrogen production, capacity factor of HPS, efficiency of WF, WF output fluctuation mitigation, and implementation.

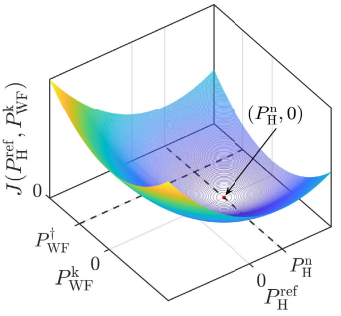


**FIGURE 6.** Three-dimensional plot of $J(P^{\mathrm{ref}}_{\mathrm{H}}, P^{\mathrm{k}}_{\mathrm{WF}})$ in (26).

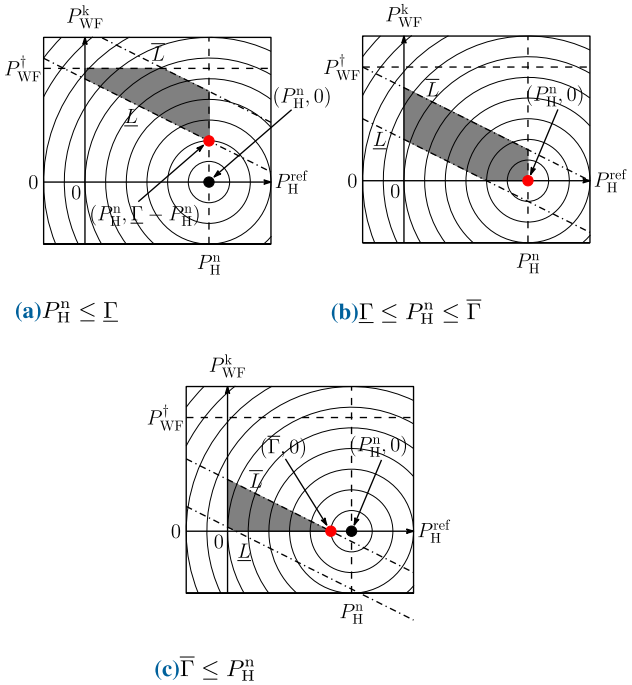


(a) $P^{\mathrm{n}}_{\mathrm{H}} \le \underline{\Gamma}$ (b) $\underline{\Gamma} \le P^{\mathrm{n}}_{\mathrm{H}} \le \overline{\Gamma}$ (c) $\overline{\Gamma} \le P^{\mathrm{n}}_{\mathrm{H}}$

**FIGURE 7.** Contour of $J(P^{\mathrm{ref}}_{\mathrm{H}}, P^{\mathrm{k}}_{\mathrm{WF}})$ in (26) and illustration of constrained optimality.

## IV. SIMULATION

We validate the proposed optimal control method by comparing it with our previous method [12] and the conventional methods proposed in [9] and [10] via simulations. The system includes a WF (500 MW) composed of five WG groups, and each group contains 20 WGs (5 MW/WG). We assume that the WGs involved in each group operate under the same wind conditions [30]. The actual wind speed data measured at a WF in Hokkaido, Japan are used. Specifically, five hard case scenarios are selected from the available wind speed data. Fig. 8 shows one scenario, and Table 3 lists the data of WF output obtained from all five. In the comparative analysis, $\eta = 0.85$. According to the technical requirement [31], we set $\gamma_h = 0.1$ and $h = 300$ s in (18). The simulation is performed on MATLAB/Simulink 2022 and the evaluation period set to $T_{\mathrm{R}} = 3600$ s. In the simulation, we use the base value $P^{\mathrm{n}}_{\mathrm{WF}} = 500$ MW in p.u. Note that the time responses for scenarios 2 to 5 are not included in this paper due to page limitations.

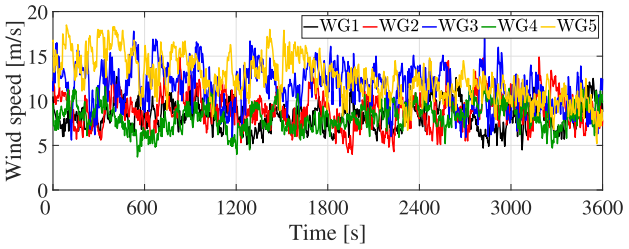


**FIGURE 8.** Wind speed (scenario 1).

**TABLE 3.** Scenario data.

| Scenario | 1 | 2 | 3 | 4 | 5 |
|---|---|---|---|---|---|
| Mean of $P_{\mathrm{WF}}$ [MW] | 275.5 | 311.5 | 220.5 | 324.5 | 280.0 |
| [a] SD of $P_{\mathrm{WF}}$ [MW] | 45.5 | 62.5 | 69.0 | 68.0 | 37.5 |
| Max. $\Delta F_{\mathrm{g}}$ [%] | 50.58 | 44.76 | 45.49 | 48.55 | 39.42 |

[a] SD: Standard deviation

**TABLE 4.** HPS specifications and controller parameters.

| | Pro. and [12] | [9] | [10] |
|---|---|---|---|
| $P_{\mathrm{H}}^{\mathrm{n}}$ [MW] | 165.9 | 185.3 | 233.5 |
| $\hat{P}_{\mathrm{H}}^{\mathrm{n}}(=\eta P_{\mathrm{H}}^{\mathrm{n}})$ [MW] | 141.0 | 157.5 | 198.5 |
| Number of ELZ modules | 64 and 50 | 84 and 50 | 90 and 50 |
| $(n_{\mathrm{s}}, n_{\mathrm{p}}, n_{\mathrm{h}})$ | $(16, 4, 50)$ | $(21, 4, 50)$ | $(30, 3, 50)$ |
| $H^{\mathrm{n}}$ [Nm$^3$/h] | 24000 | 31500 | 33750 |
| $R_0$ [$\Omega$] | 0.120 | 0.158 | 0.300 |
| $E_0$ [V] | 1523.2 | 1999.2 | 2856.0 |
| $T$ [s] | 350 | 350 | 350 |
| $T_{\mathrm{w}}$ [s] | – | – | 700 |

Table 4 lists the HPS specification for the proposed and conventional methods (See Appendix B for the design of HPS with the proposed control method). In Table 4, Pro. stands for the proposed optimal control, $T$ and $T_{\mathrm{w}}$ are controller parameters for the conventional methods. For a fair comparison, the HPS specifications in the conventional methods are best determined by trial and error (See [12] for the detailed design process).

The same HPS specifications are used for the proposed method and our previous one in [12].

Fig. 9 shows the WF output and the power supplied to the power system. Figs. 9a and 9b show that the upper part of the fluctuation of the WF output is mitigated in the proposed optimal control and our previous one in [12] because both methods utilize kinetic energy in the WGs. The upper part fluctuation ($P_{\mathrm{WF}}^{\mathrm{k}} \approx P_{\mathrm{WF}}^{\dagger} - P_{\mathrm{WF}}$) mitigated by the proposed optimal control shown in Fig. 9a is smaller than that by our previous one in [12] shown in Fig. 9b. Thus, the efficiency of WF is increased by the proposed method since the kinetic energy is evaluated explicitly in (22). The conventional methods in [9] and [10] cannot satisfy the technical requirement as described later though these methods can smooth the WF output.

Fig. 10 shows the fluctuation ratios. From Fig. 10, we can observe that the proposed method and our previous one in [12] can satisfy the technical requirement, while the conventional methods in [9] and [10] cannot guarantee it. The proposed method achieves WF output mitigation without any controller parameter tuning since it can handle the technical

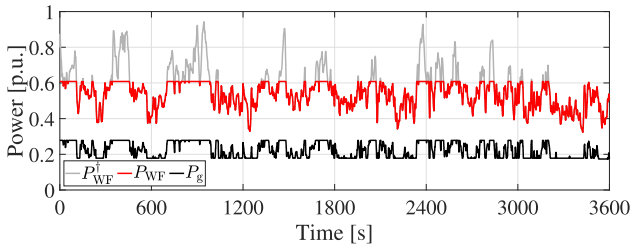


(a)Proposed optimal control method.

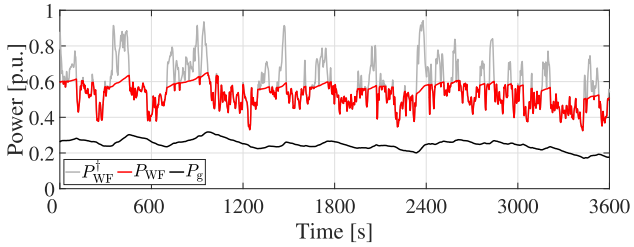


(b)Method in [12] (our previous method).

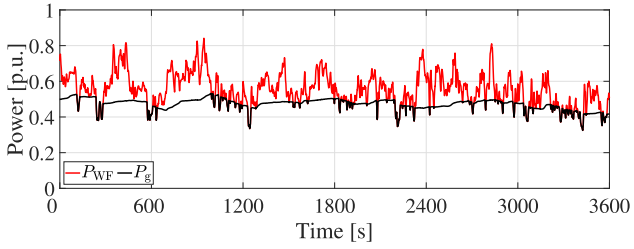


(c)Method in [9].

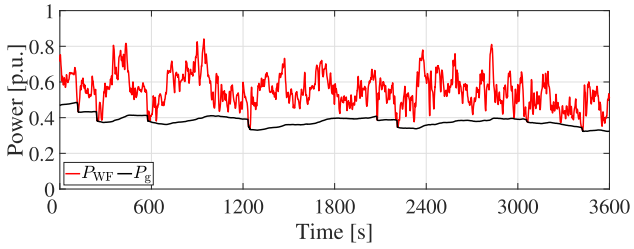


(d)Method in [10].

**FIGURE 9.** WF output and power supplied to power system.

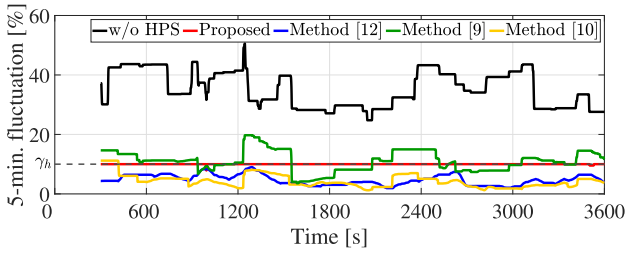


**FIGURE 10.** Fluctuation ratio $\Delta F_{\mathrm{g}}$.

requirement directly in synthesis. As a result, the proposed method can accomplish the performance of A-4.

Fig. 11 shows the consumed power in the HPSs. As shown in Figs. 11c and 11d, the HPSs with the conventional methods in [9] and [10] operate intermittently and require large-rated power to absorb the WF output fluctuations. This implies

**TABLE 5. Simulation results.**

| | Scenario 1 | | | | Scenario 2 | | | |
|---|---|---|---|---|---|---|---|---|
| | Pro. | [12] | [9] | [10] | Pro. | [12] | [9] | [10] |
| Max. $\Delta F_g$ [%] | 10 | 9.01 | 19.73 | 11.19 | 10 | 7.50 | 20.12 | 7.01 |
| Technical requirement | ✓ | ✓ | Unsatisfied | Unsatisfied | ✓ | ✓ | Unsatisfied | ✓ |
| Mean of $P_g$ [MW] | 112.0 | 123.5 | 235.0 | 190.0 | 164.9 | 152.0 | 265.0 | 210.0 |
| Hydrogen gas [$Nm^3$] | 22642 | 20495 | 5655 | 12350 | 20580 | 21145 | 6600 | 14850 |
| Capacity factor [%] | 94.3 | 85.4 | 18.0 | 36.6 | 85.8 | 88.1 | 21.0 | 44.0 |

| Scenario 3 | | | | Scenario 4 | | | | Scenario 5 | | | |
|---|---|---|---|---|---|---|---|---|---|---|---|
| Pro. | [12] | [9] | [10] | Pro. | [12] | [9] | [10] | Pro. | [12] | [9] | [10] |
| 10 | 5.34 | 15.96 | 7.25 | 10 | 8.10 | 23.83 | 17.40 | 10 | 5.96 | 14.96 | 6.28 |
| ✓ | ✓ | Unsatisfied | ✓ | ✓ | ✓ | Unsatisfied | Unsatisfied | ✓ | ✓ | Unsatisfied | ✓ |
| 59.35 | 62.5 | 182.5 | 135.0 | 149.2 | 167.0 | 275.0 | 231.5 | 114.5 | 122.5 | 243.5 | 200.0 |
| 22694 | 21410 | 5235 | 12370 | 23318 | 20860 | 6975 | 13520 | 23155 | 21265 | 5015 | 11505 |
| 94.6 | 89.2 | 16.6 | 36.7 | 97.2 | 86.9 | 22.1 | 40.1 | 96.5 | 88.6 | 15.9 | 34.1 |

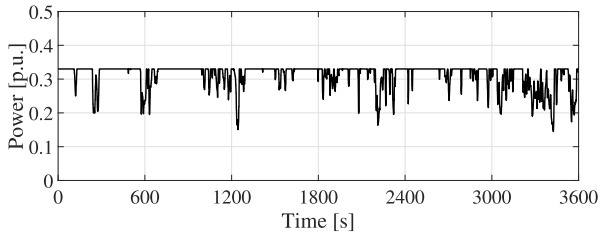


(a)Proposed optimal control method.

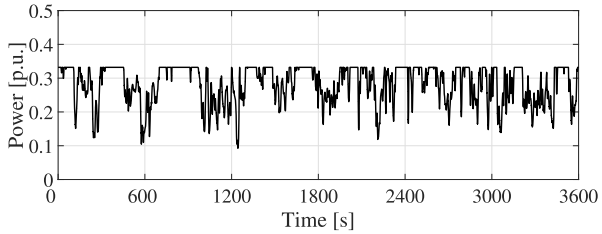


(b)Method in [12] (our previous method).

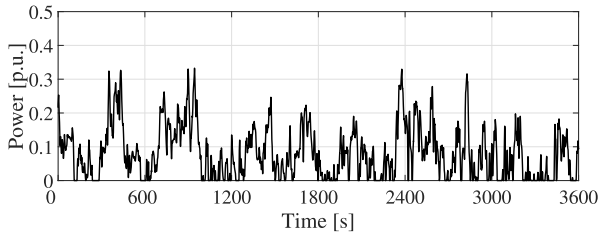


(c)Method in [9].

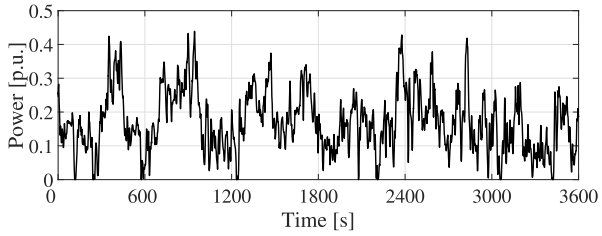


(d)Method in [10].

**FIGURE 11. Consumed power in HPS $\hat{P}_H$.**

that the low capacity factor of HPS is inevitable. By contrast, Figs. 11a and 11b demonstrate that the proposed method and our previous one in [12] can achieve a higher capacity factor of HPS than the conventional ones in [9] and [10]. Moreover,

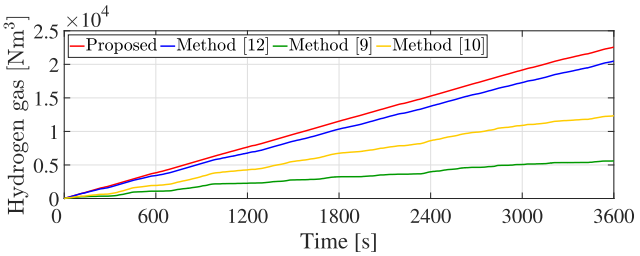


**FIGURE 12. Hydrogen gas produced in HPS.**

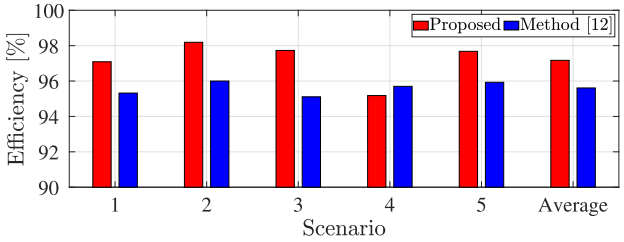


**FIGURE 13. WF efficiency in (12).**

from Figs. 11a and 11b, it can be observed that the proposed method achieves a higher capacity factor of HPS than our previous one in [12] since the proposed method optimizes the capacity factor of HPS. Thus, the performance A-2 is achieved by the proposed method.

Fig. 12 shows the hydrogen gas produced in the HPSs. As shown in Fig. 12, the HPSs with the proposed method can produce more hydrogen gas than those with the conventional methods. Fig. 12 also demonstrates that the proposed method can produce hydrogen gas constantly. In other words, the proposed method can achieve the performance of A-1.

The proposed method and our previous one in [12] utilize the kinetic energy in the WGs. Therefore, the efficiency of WF in the two methods decreases slightly. Fig. 13 shows the efficiency of WF for each scenario and the mean. It is clear from Fig. 13 that the mean of efficiency with the proposed method is 97.17%, about 1.56 point higher than that with our previous one in [12]. This evaluation implies that the proposed method can achieve the performance of A-3.

Table 5 summarizes the performance indices of the simulation results for all scenarios. The hydrogen gas obtained

**TABLE 6. Mean value of simulation results and performance indices of system.**

| | Pro. | [12] | [9] | [10] |
|---|---|---|---|---|
| Mean of $P_{\mathrm{WF}}$ [MW] | 274.2 | 270.0 | 282.5 | 282.5 |
| Mean of $P_{\mathrm{g}}$ [MW] | 120.0 | 125.5 | 240.0 | 190.0 |
| [a] Power ratio of $P_{\mathrm{g}}$ | 1 | 1.05 | 2.00 | 1.58 |
| $P_{\mathrm{H}}^{\mathrm{n}}$ [MW] | 165.9 | 165.9 | 185.3 | 233.5 |
| [b] Power ratio of $P_{\mathrm{H}}^{\mathrm{n}}$ | 1 | 1 | 1.12 | 1.41 |
| Hydrogen gas | 22478 | 21035 | 5900 | 12920 |
| [c] Hydrogen gas ratio | 1 | 0.94 | 0.26 | 0.57 |
| Capacity factor [%] | 93.7 | 87.6 | 18.7 | 38.3 |
| [d] Capacity factor ratio | 1 | 0.93 | 0.20 | 0.41 |

[a] Power ratio of $P_{\mathrm{g}} = \frac{\text{Mean of } P_{\mathrm{g}} \text{ obtained with conv. controller}}{\text{Mean of } P_{\mathrm{g}} \text{ obtained with pro. controller}}$.
[b] Power ratio of $P_{\mathrm{H}}^{\mathrm{n}} = \frac{P_{\mathrm{H}}^{\mathrm{n}} \text{ of HPS with conv. controller}}{P_{\mathrm{H}}^{\mathrm{n}} \text{ of HPS with pro. controller}}$.
[c] Hydrogen gas ratio $= \frac{\text{Hydrogen gas produced by HPS with conv. controller}}{\text{Hydrogen gas produced by HPS with pro. controller}}$.
[d] Capacity factor ratio $= \frac{\text{Capacity factor of HPS with conv. controller}}{\text{Capacity factor of HPS with pro. controller}}$.

with the proposed method is the highest among the control methods. Moreover, the proposed method can achieve the highest capacity factor of HPS among the control methods. The proposed method and our previous one in [12] also satisfy the technical requirement for all scenarios without high-rated-power HPSs, as listed in Table 5. Furthermore, the WF operated by the proposed method can achieve higher efficiency than that by our previous one in [12]. The mean of $P_{\mathrm{g}}$ obtained by the proposed optimal control method is smaller than that obtained by the conventional methods. Nevertheless, the proposed method allows us to introduce a large-scale WF to power systems because it satisfies the technical requirement.

From the simulation results, it can be concluded that the proposed optimal control method can produce hydrogen constantly, keeping the high capacity factor of HPS, achieving a high efficiency of WF utilizing kinetic energy, and satisfying the technical requirement.

## V. CONCLUSION

In this paper, we proposed a novel optimal control method for the integrated system of WF and HPS. Optimal output references to increase the capacity factor of HPS and the efficiency of WF can be obtained by the proposed method without complex calculation.

Comparative simulation analysis with the proposed and conventional methods showed that the proposed method could satisfy the technical requirement by smoothing WF output fluctuations sufficiently while keeping a high capacity factor of HPS. It was validated from the simulation results that the proposed method was significantly effective for the integrated system of the WF and the HPS.

## APPENDIX

### A. DERIVATION OF (22)

We define $\overline{\alpha}[k;\hat{h}]$ and $\underline{\alpha}[k;\hat{h}]$ as follows:

$$\overline{\alpha}[k;\hat{h}] = \max_{k-\hat{h}\le\kappa<k} P_{\mathrm{g}}[\kappa], \tag{31}$$

$$\underline{\alpha}[k;\hat{h}] = \min_{k-\hat{h}\le\kappa<k} P_{\mathrm{g}}[\kappa]. \tag{32}$$

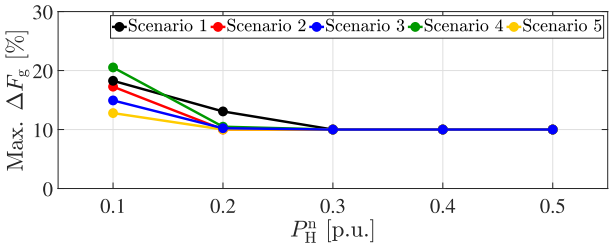


**FIGURE 14. Maximum of $\Delta F_{\mathrm{g}}$ vs. $P_{\mathrm{H}}^{\mathrm{n}}$.**

From (19), (20), (31), and (32), we obtain

$$\max(P_{\mathrm{g}}[k], \overline{\alpha}[k;\hat{h}]) - \min(P_{\mathrm{g}}[k], \underline{\alpha}[k;\hat{h}]) \le \gamma_h \cdot P_{\mathrm{WF}}^{\mathrm{n}}. \tag{33}$$

Considering $\overline{\alpha}[k;\hat{h}] - \underline{\alpha}[k;\hat{h}] < \gamma_h \cdot P_{\mathrm{WF}}^{\mathrm{n}}$ and $\overline{\alpha}[k;\hat{h}] \ge \underline{\alpha}[k;\hat{h}]$, we can rewrite (33) as

$$\begin{cases} P_{\mathrm{g}}[k] - \underline{\alpha}[k;\hat{h}] \le \gamma_h \cdot P_{\mathrm{WF}}^{\mathrm{n}} & (P_{\mathrm{g}}[k] \ge \overline{\alpha}[k;\hat{h}]), \\ \overline{\alpha}[k;\hat{h}] - P_{\mathrm{g}}[k] \le \gamma_h \cdot P_{\mathrm{WF}}^{\mathrm{n}} & (\underline{\alpha}[k;\hat{h}] \ge P_{\mathrm{g}}[k]). \end{cases} \tag{34}$$

We define $\underline{\Gamma}[k;\hat{h},\gamma_h]$ and $\overline{\Gamma}[k;\hat{h},\gamma_h]$ as follows:

$$\underline{\Gamma}[k;\hat{h},\gamma_h] = P_{\mathrm{WF}}^{\dagger}[k] - \gamma_h \cdot P_{\mathrm{WF}}^{\mathrm{n}} - \underline{\alpha}[k;\hat{h}], \tag{35}$$

$$\overline{\Gamma}[k;\hat{h},\gamma_h] = P_{\mathrm{WF}}^{\dagger}[k] + \gamma_h \cdot P_{\mathrm{WF}}^{\mathrm{n}} - \overline{\alpha}[k;\hat{h}]. \tag{36}$$

From (34) and $P_{\mathrm{g}} \approx P_{\mathrm{WF}}^{\dagger} - P_{\mathrm{WF}}^{\mathrm{k}} - P_{\mathrm{H}}$, we obtain (21).

### B. DESIGN OF HPS

We investigate $P_{\mathrm{H}}^{\mathrm{n}}$ with which the HPS can smooth the WF output sufficiently. Fig. 14 shows the maximum $\Delta F_{\mathrm{g}}$ vs. $P_{\mathrm{H}}^{\mathrm{n}}$. Note that the base value is $P_{\mathrm{WF}}^{\mathrm{n}} = 500$ MW in p.u. It is clear from Fig. 14 that the grid code ($\Delta F_{\mathrm{g}} < 10$ %) is satisfied when $P_{\mathrm{H}}^{\mathrm{n}} > 0.3$. In our previous method [12], the technical requirement is satisfied when $P_{\mathrm{H}}^{\mathrm{n}} > 0.33$. For a fair comparison, as listed in Table 4, $P_{\mathrm{H}}^{\mathrm{n}}$ is shared with our previous method [12].

## REFERENCES

[1] L. Sun, G. Wu, Y. Xue, J. Shen, D. Li, and K. Y. Lee, "Coordinated control strategies for fuel cell power plant in a microgrid," *IEEE Trans. Energy Convers.*, vol. 33, no. 1, pp. 1–9, Mar. 2018.
[2] A. Chapman, D. H. Nguyen, H. Farabi-Asl, K. Itaoka, K. Hirose, and Y. Fujii, "Hydrogen penetration and fuel cell vehicle deployment in the carbon constrained future energy system," *IET Electr. Syst. Transp.*, vol. 10, no. 4, pp. 409–416, Dec. 2020.
[3] T. Rudolf, T. Schurmann, S. Schwab, and S. Hohmann, "Toward holistic energy management strategies for fuel cell hybrid electric vehicles in heavy-duty applications," *Proc. IEEE*, vol. 109, no. 6, pp. 1094–1114, Jun. 2021.
[4] *Global Offshore Wind Report 2020 [R]*, Global Wind Energy Council, Brussels, Belgium, 2020.
[5] Y.-S. Huang and S.-J. Liu, "Chinese green hydrogen production potential development: A provincial case study," *IEEE Access*, vol. 8, pp. 171968–171976, 2020.
[6] K. Zhang, B. Zhou, S. W. Or, C. Li, C. Y. Chung, and N. Voropai, "Optimal coordinated control of multi-renewable-to-hydrogen production system for hydrogen fueling stations," *IEEE Trans. Ind. Appl.*, vol. 58, no. 2, pp. 2728–2739, Mar. 2022.

[7] A. Khalilnejad, A. Sundararajan, and A. I. Sarwat, "Optimal design of hybrid wind/photovoltaic electrolyzer for maximum hydrogen production using imperialist competitive algorithm," *J. Modern Power Syst. Clean Energy*, vol. 6, no. 1, pp. 40–49, Jan. 2018.
[8] F. Alonge, S. M. Collura, F. D'Ippolito, D. Guilbert, M. Luna, and G. Vitale, "Design of a robust controller for DC/DC converter–electrolyzer systems supplied by $\mu$WECSs subject to highly fluctuating wind speed," *Control Eng. Pract.*, vol. 98, May 2020, Art. no. 104383.
[9] R. Takahashi, H. Kinoshita, T. Murata, J. Tamura, M. Sugimasa, A. Komura, M. Futami, M. Ichinose, and K. Ide, "Output power smoothing and hydrogen production by using variable speed wind generators," *IEEE Trans. Ind. Electron.*, vol. 57, no. 2, pp. 485–493, Feb. 2010.
[10] A. Takahashi, A. Goto, Y. Machida, and S. Funabiki, "A power smoothing control method for a photovoltaic generation system using a water electrolyzer and its filtering characteristics," *Electr. Eng. Jpn.*, vol. 206, no. 2, pp. 25–32, Jan. 2019.
[11] P. Zhao, C. Gu, Z. Hu, D. Xie, I. Hernando-Gil, and Y. Shen, "Distributionally robust hydrogen optimization with ensured security and multi-energy couplings," *IEEE Trans. Power Syst.*, vol. 36, no. 1, pp. 504–513, Jan. 2021.
[12] K. Koiwa, L. Cui, T. Zanma, K.-Z. Liu, and J. Tamura, "A coordinated control method for integrated system of wind farm and hydrogen production: Kinetic energy and virtual discharge controls," *IEEE Access*, vol. 10, pp. 28283–28294, 2022.
[13] S. G. Tesfahunegn, Ø. Ulleberg, P. J. Vie, and T. M. Undeland, "PV fluctuation balancing using hydrogen storage—A smoothing method for integration of PV generation into the utility grid," *Energy Proc.*, vol. 12, pp. 1015–1022, Jan. 2011.
[14] T. Zhou and B. Francois, "Energy management and power control of a hybrid active wind generator for distributed power generation and grid integration," *IEEE Trans. Ind. Electron.*, vol. 58, no. 1, pp. 95–104, Jan. 2011.
[15] D. F. Recalde Melo and L.-R. Chang-Chien, "Synergistic control between hydrogen storage system and offshore wind farm for grid operation," *IEEE Trans. Sustain. Energy*, vol. 5, no. 1, pp. 18–27, Jan. 2014.
[16] T. Wen, Z. Zhang, X. Lin, Z. Li, C. Chen, and Z. Wang, "Research on modeling and the operation strategy of a hydrogen-battery hybrid energy storage system for flexible wind farm grid-connection," *IEEE Access*, vol. 8, pp. 79347–79356, 2020.
[17] F. Garcia-Torres and C. Bordons, "Optimal economical schedule of hydrogen-based microgrids with hybrid storage using model predictive control," *IEEE Trans. Ind. Electron.*, vol. 62, no. 8, pp. 5195–5207, Aug. 2015.
[18] X. Chen, W. Cao, Q. Zhang, S. Hu, and J. Zhang, "Artificial intelligence-aided model predictive control for a grid-tied wind-hydrogen-fuel cell system," *IEEE Access*, vol. 8, pp. 92418–92430, 2020.
[19] *Global Wind Report 2021 [R]*, Global Wind Energy Council, Brussels, Belgium, 2021.
[20] M. Rosyadi, A. Umemura, R. Takahashi, J. Tamura, N. Uchiyama, and K. Ide, "Simplified model of variable speed wind turbine generator for dynamic simulation analysis," *IEEJ Trans. Power Energy*, vol. 135, no. 9, pp. 538–549, 2015.
[21] M. Rosyadi, S. M. Muyeen, R. Takahashi, and J. Tamura, "New controller design for PMSG based wind generator with LCL-filter considered," in *Proc. XXth Int. Conf. Electr. Mach.*, Sep. 2012, pp. 2112–2118.
[22] S. G. Varzaneh, G. B. Gharehpetian, and M. Abedi, "Output power smoothing of variable speed wind farms using rotor-inertia," *Electr. Power Syst. Res.*, vol. 116, pp. 208–217, Nov. 2014.
[23] K. Koiwa, T. Tawara, M. Watanabe, K.-Z. Liu, T. Zanma, and J. Tamura, "Novel cost reduction method for wind farms associated with energy storage systems by optimal kinetic energy control," *Appl. Sci.*, vol. 10, no. 20, p. 7223, Oct. 2020.
[24] H. Jun and I. Tatsuhiko, "A high-purity hydrogen and oxygen generator (HHOG) for ghemical industry," *Tech. Document Shinkou Pantetuku*, vol. 40, no. 2, pp. 48–56, Mar. 1997.
[25] J. Koponen, V. Ruuskanen, A. Kosonen, M. Niemela, and J. Ahola, "Effect of converter topology on the specific energy consumption of alkaline water electrolyzers," *IEEE Trans. Power Electron.*, vol. 34, no. 7, pp. 6171–6182, Jul. 2019.
[26] F. J. Pino, L. Valverde, and F. Rosa, "Influence of wind turbine power curve and electrolyzer operating temperature on hydrogen production in wind–hydrogen systems," *J. Power Sources*, vol. 196, no. 9, pp. 4418–4426, May 2011.
[27] C.-L. Nguyen and H.-H. Lee, "Power management approach to minimize battery capacity in wind energy conversion systems," *IEEE Trans. Ind. Appl.*, vol. 53, no. 5, pp. 4843–4854, Sep. 2017.
[28] K. Koiwa, T. Ishii, K.-Z. Liu, T. Zanma, and J. Tamura, "One-sample optimal output smoothing method for wind farm with energy storage system," *IET Renew. Power Gener.*, vol. 15, no. 3, pp. 653–663, 2021.
[29] M. Jannati, S. H. Hosseinian, B. Vahidi, and G.-J. Li, "Mitigation of wind-farm power fluctuation by adaptive linear neuron-based power tracking method with flexible learning rate," *IET Renew. Power Gener.*, vol. 8, no. 6, pp. 659–669, 2014.
[30] Z. Guo and W. Wu, "Data-driven model predictive control method for wind farms to provide frequency support," *IEEE Trans. Energy Convers.*, vol. 37, no. 2, pp. 1304–1313, Jun. 2022.
[31] Kansai Electric Power Company. (2022). *Grid Interconnection Technical Requirement*. Accessed: Oct. 19, 2022. [Online]. Available: https://www.kansai-td.co.jp/consignment/agreement/pdf/20220701_ktrenkei_dt.pdf

**KENTA KOIWA** (Member, IEEE) was born in 1989. He received the B.E. and M.E. degrees in electrical engineering from the Kitami Institute of Technology, Japan, in 2012 and 2014, respectively, and the Ph.D. degree in electrical engineering from Chiba University, Japan, in 2017.

Since 2017, he has been an Assistant Professor with the Department of Electrical and Electronic Engineering, Chiba University. His research interests include power systems, renewable energy, and power electronics.

**LINMAN CUI** received the B.E. degree in electrical engineering from the China University of Petroleum, Qingdao, China, in 2016. She is currently pursuing the M.E. degree in electrical engineering with Chiba University, Japan.

Her research interest includes wind power output smoothing.

**TADANAO ZANMA** (Member, IEEE) was born in 1972. He received the B.S., M.S., and Dr. (Eng.) degrees from Nagoya University, in 1995, 1997, and 2000, respectively, all in electrical engineering.

From 2000 to 2007, he was with Mie University initially as a Research Associate, and since 2007, he has been an Assistant Professor. In 2007, he was an Academic Guest at ETH Zurich. He was an Associate Professor at Mie University, from 2009 to 2011. He has been with Chiba University as an Associate Professor, since 2011. His current research interests include hybrid dynamical control, switched systems, and networked control systems, especially system control based on mixed logical dynamical systems and model predictive control.

Dr. Zanma has received FANUC FA and Robot Foundation Thesis Prize, in 2009, and IEEJ Distinguished Paper Award 2010 and 2015.

**KANG-ZHI LIU** (Senior Member, IEEE) received the B.E. degree in aeronautic engineering from Northwestern Polytechnical University, China, in 1984, and the M.E. and Ph.D. degrees in electrical engineering from Chiba University, Chiba, Japan, in 1988 and 1991, respectively.

Then, he joined Chiba University and currently a Professor. He has authored six books. His research interests include control theory, power systems, smart grids, and electrical drives.

Dr. Liu was a recipient of the Young Author Award and three best paper awards from the Society of Instrument and Control Engineers (SICE), Japan. He was the Director and the Executive Director of SICE, in 2017 and 2018, respectively.